Schottky effect in the *i*-Zn-Ag-Sc-Tm icosahedral quasicrystal and its 1/1 Zn-Sc-Tm approximant

S. Jazbec,[1] S. Kashimoto,[2] P. Koželj,[1] S. Vrtnik,[1] M. Jagodič,[3] Z. Jagličić,[3] and J. Dolinšek[1,*]

[1]*J. Stefan Institute and University of Ljubljana, Faculty of Mathematics and Physics, Jamova 39, SI-1000 Ljubljana, Slovenia*

[2]*Division of Applied Physics, Graduate School of Engineering, Hokkaido University, Kita-ku, 060-8628 Sapporo, Japan*

[3]*Institute of Mathematics, Physics and Mechanics and University of Ljubljana, Faculty of Civil and Geodetic Engineering, Jadranska 19, SI-1000 Ljubljana, Slovenia*

(Received 13 July 2015; revised manuscript received 4 February 2016; published 23 February 2016)

The analysis of low-temperature specific heat of rare-earth (RE)-containing quasicrystals and periodic approximants and consequent interpretation of their electronic properties in the $T \to 0$ limit is frequently hampered by the Schottky effect, where crystalline electric fields lift the degeneracy of the RE-ion Hund's rule ground state and introduce additional contribution to the specific heat. In this paper we study the low-temperature specific heat of a thulium-containing *i*-Zn-Ag-Sc-Tm icosahedral quasicrystal and its 1/1 Zn-Sc-Tm approximant, both being classified as "Schottky" systems. We have derived the crystal-field Hamiltonian for pentagonal symmetry of the crystalline electric field, pertinent to the class of Tsai-type icosahedral quasicrystals and their approximants, where the RE ions are located on fivefold axes of the icosahedral atomic cluster. Using the leading term of this Hamiltonian, we have calculated analytically the Schottky specific heat in the presence of an external magnetic field and made comparison to the experimental specific heat of the investigated quasicrystal and approximant. When the low-temperature specific heat C is analyzed in a C/T versus T^2 scale (as it is customarily done for metallic specimens), the Schottky specific heat yields an upturn in the $T \to 0$ limit that cannot be easily distinguished from a similar upturn produced by the electron-electron interactions in exchange-enhanced systems and strongly correlated systems. Our results show that extraction of the electronic properties of RE-containing quasicrystals from their low-temperature specific heat may be uncertain in the presence of the Schottky effect.

DOI: 10.1103/PhysRevB.93.054208

I. INTRODUCTION

When studying fundamental physics of solid materials containing rare-earth (RE) elements, there is a drawback which often hampers the interpretation of low-temperature experimental data, namely the crystal-field (CF) splitting of the Hund's rule ground state [1]. In a solid, the highly anisotropic $4f$ charge cloud of a RE ion interacts with the crystalline electric field and lifts the $(2J+1)$-fold degeneracy of the RE-ion ground state with the total angular momentum $\hbar\vec{J}$, producing a set of discrete energy levels (here gadolinium is an exception, because its charge cloud is spherically symmetric and the CF interaction is zero). Specific heat of a system with discrete energy levels possesses an additional contribution that becomes dominant at low temperatures, known as the Schottky effect [2]. The Schottky specific heat C_{Sch} is characterized by a broad peak, appearing at a temperature that is a fraction of the energy difference $\Delta\varepsilon/k_B$ (in temperature units) between the CF-split energy levels. For small CF splittings, the peak may appear in the Kelvin or sub-Kelvin temperature range, where it obscures the electronic specific heat of a metallic specimen. Precise determination of the electronic specific heat coefficient γ may thus be difficult and uncertain for metallic samples containing RE elements. In addition, when the low-temperature total specific heat of a RE-containing metallic alloy is presented in a C/T versus T^2 scale (as it is customary done), the Schottky specific heat term yields an upturn in the $T \to 0$ limit that cannot be easily distinguished from a similar upturn produced by the electron-electron interactions in exchange-enhanced systems and strongly correlated systems. The low-temperature magnetic susceptibility can also be affected by the CF effects [1,3,4]. The CF-split energy level scheme of some RE ions contains a nonmagnetic ground state, whereas higher levels are magnetic. In the $T \to 0$ limit, the weight of the nonmagnetic state in the electronic magnetization increases, so that the magnetic susceptibility χ decreases. In a χ^{-1} versus T diagram, a Curie-Weiss-like deviation from the linear $\chi^{-1} \propto T$ Curie behavior is observed at low temperatures and an effective Curie-Weiss temperature may be defined. However, both the CF-induced Curie-Weiss behavior of the susceptibility and the Schottky specific heat are single-ion properties, depending on the distribution of electric charges around the RE ion, but are not related to the interactions within the electronic system. Special care should be taken when analyzing the electronic and magnetic properties of a metallic system containing RE elements on the basis of its low-temperature specific heat and magnetic susceptibility.

The difficulty in ascertaining the CF splitting is twofold. First, a proper CF Hamiltonian has to be evaluated, and second, the CF parameters, which parametrize the CF Hamiltonian, have to be determined either by appropriate models or by experiment. In metallic compounds, the CF parameters have to be supplied solely by the experiment, because the conduction electrons make significant contribution to the CF splitting, for which no predictive models exist and the point-charge model does not apply. The CF splitting schemes have been derived for certain crystal symmetries by group-theoretical methods and the introduction of Stevens' equivalent operators O_n^m, tabulated by various authors [5,6]. For cubic [7] and hexagonal [8–12] symmetries, the CF-split energy-level schemes have been published for all RE ions.

The case of icosahedral symmetry has been considered by Walter [13,14]. Icosahedral symmetry represents the

*Corresponding author: jani.dolinsek@ijs.si

highest point symmetry in three dimensions and is found in icosahedral quasicrystals (i-QCs), where icosahedral atomic clusters represent the basic building block of the structure. Icosahedral nearest-neighbor coordination is also considered to exist in metallic glasses, giving rise to a maximum local mass density. The CF-split energy level schemes for all RE ions were published for a special case where the RE ion feels the electrostatic potential of ideal icosahedral symmetry [13], i.e., the RE ion is located in the center of a regular icosahedron with equal charges at its 12 vertices. In real i-QCs, this highly symmetric case has never been encountered. Most of the so-far known RE-containing i-QCs belong to the class of Tsai-type quasicrystals, possessing the structure of the i-$Cd_{5.7}Yb$ parent compound that can be described as a packing of interpenetrating rhombic triacontahedral, or Tsai-type atomic clusters [15–17]. A rhombic triacontahedral cluster contains inside a three-shell icosahedral cluster, consisting of an inner dodecahedron, a middle icosahedron, and an outer icosidodecahedron. The RE atoms are located at the vertices of the middle icosahedron and their first coordination shell does not possess icosahedral symmetry, so that the published CF schemes in an icosahedral field do not apply. However, the local near-neighbor atomic environment of these RE atoms possesses fivefold symmetry, as a consequence of the fact that the RE atoms are located on fivefold axes of the icosahedron. In this paper we first elaborate theoretically the CF effects for the electrostatic potential of pentagonal (fivefold) rotational symmetry, applicable to the class of Tsai-type i-QCs and their periodic approximants that contain the same three-shell icosahedral cluster as a backbone of the structure (here it should be noted that the Cd_6Yb-type approximants possess an additional small tetrahedron in the center of the three-shell cluster that breaks its overall icosahedral symmetry [17]). Experimentally we demonstrate the CF effects for the i-Zn-Ag-Sc-Tm Tsai-type icosahedral quasicrystal and its 1/1 Zn-Sc-Tm cubic approximant. We show that the CF-split energy levels of thulium ions introduce Schottky contribution to the specific heat that exhibits a broad maximum at a temperature around 1 K and the maximum is shifted to higher temperatures by the application of an external magnetic field. In addition, we demonstrate that the nuclear Schottky effect, being much weaker than the ionic Schottky effect, is also observed experimentally in the specific heat of the i-Zn-Ag-Sc-Tm and 1/1 Zn-Sc-Tm at sub-Kelvin temperatures. The presence of Schottky effect greatly aggravates extraction of the electronic properties of RE-containing quasicrystals and their approximants in the $T \to 0$ limit from the low-temperature specific heat.

II. STRUCTURAL ANALYSIS

The i-$Cd_{5.7}Yb$ (or i-$Cd_{85}Yb_{15}$ in at. %) prototype structure [17] of the Tsai-type i-QCs is realized in many alloy systems by replacing the majority element cadmium with Zn or combinations Zn-M (M = Mg, Cu, Pd, Ag, Pt, Au), Zn-T (T = Mn, Fe, Co, Ni), Cu-Al, Cu-Ga, Cd-Mg, Ag-Al, Ag-In, Pd-Al, Au-Al, Au-Ga, and Au-In, whereas the minor component can be trivalent transition elements such as Sc, Y or lanthanides, or divalent Ca or Yb [18–20]. In all cases, composition of the minor component ranges from 12 to 16 at. %, and the Tsai-type QCs satisfy an almost constant valence-electron concentration per atom e/a, ranging from 2.00 to 2.15. Among these, the following RE-containing i-QCs were reported: i-Ag-In-(Gd,Yb) [21,22], i-Au-(Al,In)-Yb [20,23,24], i-Zn-Fe-Sc-(Ho,Er,Tm) [25], i-Zn-Ag-Sc-Tm (this work), and the newly discovered binary group i-$Cd_{7.55}RE$ with RE = Gd, Tb, Dy, Ho, Er, and Tm [26]. The only known RE-containing i-QCs that do not belong to the Tsai class are those from the i-(Zn,Cd)-Mg-RE series [27,28], which are structurally based on the Bergman type (or Frank-Kasper type) icosahedral cluster. Periodic approximants of the Tsai-type i-QCs possess the $Zn_{17}Sc_3$ ($Zn_{85}Sc_{15}$) body-centered cubic (bcc) structure [29] and the reported RE-containing approximants include 1/1 Cd_6Yb [30], 2/1 $Cd_{5.8}Yb$ [31], 1/1 $(Ce,Gd)_{15}Au_{65}Sn_{20}$ [32,33], 1/1 $Zn_{85.5}Sc_{11}Tm_{3.5}$ (this work), 1/1 $Ag_{40}In_{46}Yb_{14}$ [34], and 2/1 $Ag_{41}In_{44}Yb_{15}$ [35]. There is a slight difference in the distribution of the RE atoms within the structures of the i-QCs and their approximants. In the approximants, all RE atoms are located exclusively on the middle icosahedron of the basic three-shell cluster (i.e., there is only one RE crystallographic site), while in the i-QCs, about 70% of RE atoms are located on the icosahedra, whereas the remaining 30% are found in the glue that fills the gaps between the clusters.

The local atomic coordination around the RE atom located on the icosahedron of the three-shell cluster, which determines its CF Hamiltonian, will be presented for the structural model of the 1/1 $Ce_{15}Au_{65}Sn_{20}$ bcc approximant (space group $Im\bar{3}$, $a = 1.5190$ nm, 161 atoms in the unit cell) [32] a representative member of the Tsai-type approximants. The reason why we have chosen the ternary 1/1 $Ce_{15}Au_{65}Sn_{20}$ approximant for the analysis instead of the binary 1/1 Zn-Sc approximant that is more closely related to the investigated 1/1 Zn-Sc-Tm (for which the structural model has not yet been determined) is the fact that $Ce_{15}Au_{65}Sn_{20}$ better illustrates the distribution of three chemical elements and the associated chemical disorder on the three-shell cluster, whereas in the case of the 1/1 Zn-Sc no chemical disorder exists. The structure of the 1/1 $Ce_{15}Au_{65}Sn_{20}$ can be described by a periodic arrangement of the three-shell icosahedral clusters, located at the nodes of the bcc unit cell, as shown in Fig. 1(a). One such cluster is shown in Fig. 1(b). The inner shell is a 20-atom dodecahedron decorated by 12 Au and 8 Sn atoms at 0.39 nm from the bcc nodes. The second shell is a perfect icosahedron decorated by 12 Ce atoms at 0.54 nm. The third shell is an icosidodecahedron decorated by 30 Au atoms at 0.61 nm. The glue atoms, located between the clusters, are either gold or tin atoms.

The nearest-neighbor atomic coordination around a given Ce atom, including atoms up to the maximum distance $r = 0.35$ nm, is shown as a side view in Fig. 1(c) and along the fivefold axis in Fig. 1(d). The fivefold axis, passing from the three-shell cluster center through the Ce atom, is marked by a dashed line. Within this nearest-neighbor coordination sphere, there are 16 atoms surrounding the central Ce atom, 15 of them forming three more or less regular pentagons, whereas the 16th atom is located on the fivefold axis. The atomic distribution around a Ce atom thus shows pentagonal (fivefold) rotational symmetry. The bottom pentagon (the one closest to the three-shell cluster center) is formed from atoms

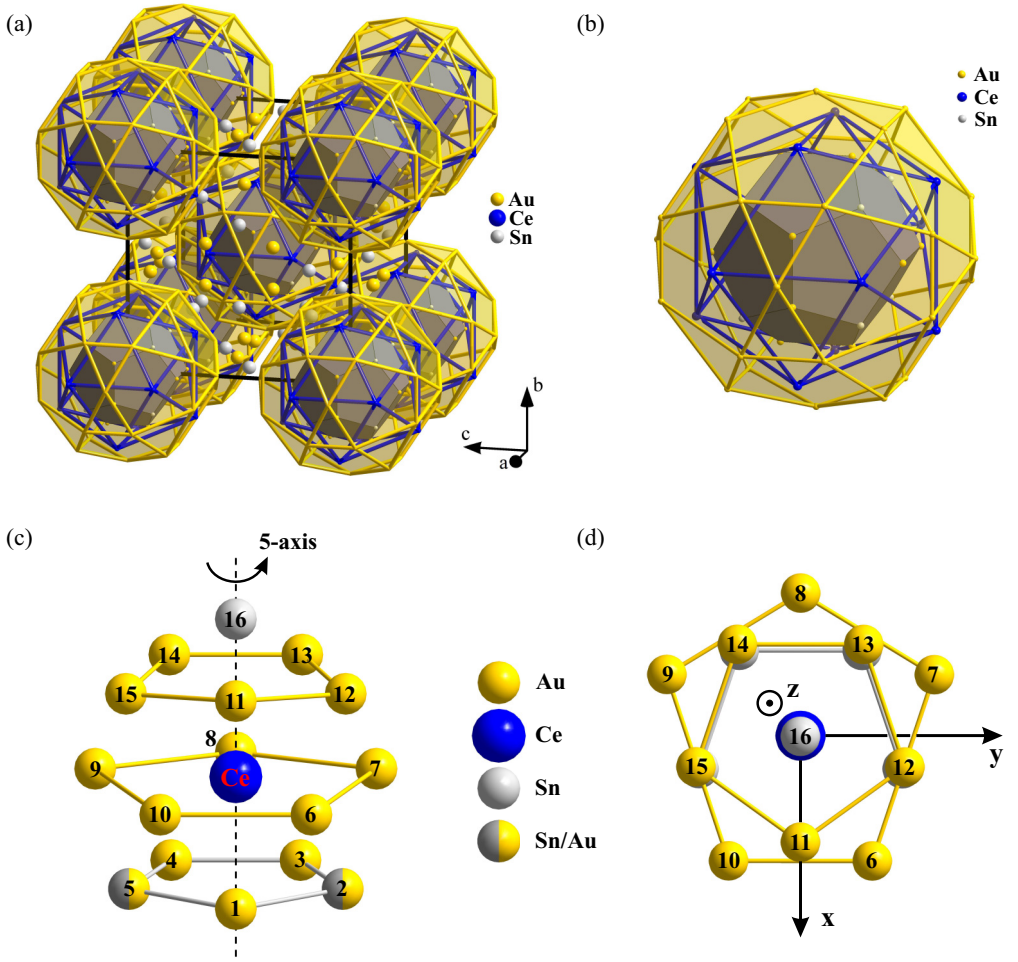

FIG. 1. (a) Unit cell of the $Ce_{15}Au_{65}Sn_{20}$ Tsai-type 1/1 bcc approximant according to the structural model by Kenzari *et al.* [32]. The structure can be described by a periodic arrangement of three-shell atomic clusters with icosahedral symmetry, located at the nodes of the bcc unit cell. (b) A three-shell icosahedral cluster on an expanded scale. The inner shell is an $(Sn, Au)_{20}$ dodecahedron (gray online), the middle shell is a Ce_{12} icosahedron (blue online), and the outer shell is an Au_{30} icosidodecahedron (yellow). (c) The nearest-neighbor atomic coordination shell around a given Ce atom, shown in a side view. The fivefold axis, passing from the three-shell cluster center through the Ce atom, is marked by a dashed line. (d) A view of the nearest-neighbor coordination shell along the fivefold axis.

labeled 1–5, belonging to the inner dodecahedron (mixed Au and Sn, yellow/gray-colored online). The middle pentagon is formed from gold atoms (6–10, yellow) belonging to the outer icosidodecahedron. The top pentagon is formed from gold atoms (11–15, yellow) that belong to the icosidodecahedron of the adjacent three-shell cluster and the glue atoms. Atom 16 is Sn (gray), located on a fivefold axis. The next-nearest neighbor atoms (outside of the first coordination shell) are located at distances >0.40 nm from the Ce atom, but again form pentagons around the fivefold axis, with the exception of two split atomic positions. The distance of the central Ce atom to the nearest Ce neighbors on the icosahedral shell is quite large, amounting to $r_{Ce-Ce} \approx 0.57$ nm (the closest Ce neighbors on the adjacent three-shell cluster are at about the same distance).

III. THE CF HAMILTONIAN

The CF Hamiltonian will now be derived under the assumption that the RE ion feels the electrostatic potential of pentagonal (fivefold) rotational symmetry. Our derivation follows the works of Hutchings [5] and Walter [13]. The Hamiltonian of the RE ion in a crystal is of the form $\mathcal{H} = \mathcal{H}_0 + V_{CF}$, where $\mathcal{H}_0$ is the Hamiltonian of the free ion and V_{CF} is the electrostatic potential energy of the ion in the crystal electric field of the neighboring charges, which has the symmetry of the local surroundings. The CF potential V_{CF} can be expanded in terms of tesseral (real) harmonics $Z_{nm}(\theta,\phi)$ (electrical multipoles) [5] which form an orthonormal set of functions

$$V_{CF}(r,\theta,\phi) = \sum_{n=0}^{6}\sum_{m=0}^{n} r^n \gamma_{nm} Z_{nm}(\theta,\phi), \qquad (1)$$

with n even and m a multiple of p, where p stands for the p-fold symmetry ($p = 5$ in our case) along the z axis of an arbitrary reference frame, and (r,θ,ϕ) denote polar coordinates. The coefficients γ_{nm} are

$$\gamma_{nm} = \sum_j \frac{4\pi}{2n+1} q_j \frac{Z_{nm}(\theta_j,\phi_j)}{R_j^{n+1}}, \qquad (2)$$

where q_j and (R_j,θ_j,ϕ_j) are the charge and the location of the jth atom with respect to the RE ion. For the fivefold-symmetric distribution of charges around the RE ion, $V_{\rm CF}$ can be written as (by omitting the $n = 0$ term, which shifts the energy levels but does not affect their CF splittings)

$$V_{\rm CF}(r,\theta,\phi) = r^2\gamma_{20}Z_{20}(\theta,\phi) + r^4\gamma_{40}Z_{40}(\theta,\phi) + r^6\gamma_{60}Z_{60}(\theta,\phi) + r^6\gamma_{65}Z_{65}(\theta,\phi). \quad (3)$$

The following tesseral harmonics appear in Eq. (3):

$$Z_{20} = \frac{1}{4}\sqrt{\frac{5}{\pi}}(3\cos^2\theta - 1), \quad (4a)$$

$$Z_{40} = \frac{3}{16}\sqrt{\frac{1}{\pi}}(35\cos^4\theta - 30\cos^2\theta + 3), \quad (4b)$$

$$Z_{60} = \frac{1}{32}\sqrt{\frac{13}{\pi}}(231\cos^6\theta - 315\cos^4\theta + 105\cos^2\theta - 5), \quad (4c)$$

$$Z_{65} = \frac{3}{32}\sqrt{\frac{2002}{\pi}}\cos\theta\sin^5\theta\cos 5\phi. \quad (4d)$$

The expansion of $V_{\rm CF}$ given by Eq. (3) is equally valid for the icosahedral symmetry [13] since the RE ion in the center of an icosahedron is located on a fivefold axis. For the ideal icosahedral symmetry, where equal charges $q_j = q_0$ are located at the 12 vertices of the icosahedron at distances $R_j = R_0$ from the central RE atom, it is straightforward to show that the coefficients γ_{20} and γ_{40} vanish due to the high symmetry and Z_{60} and Z_{65} are the only contributing multipole terms in Eq. (3) [13]. Using the Stevens's "operator equivalents" technique [36], the electrical multipoles Z_{nm} are transformed into the corresponding total angular momentum representations, the CF operators $O_n^m(J)$. Thereby the Z_{nm} are multiplied with the charge of one electron e and summed over all $4f$ electrons, thus transforming the CF potential $V_{\rm CF}$ into a CF Hamiltonian $\mathcal{H}_{\rm CF}$. The icosahedral CF Hamiltonian $\mathcal{H}_{\rm CF}^{\rm ico}$ is then given by [13]

$$\mathcal{H}_{\rm CF}^{\rm ico} = B_6\left(O_6^0 - 42O_6^5\right), \quad (5)$$

where

$$B_6 = A_6\gamma_J\langle r^6\rangle, \quad (6)$$

and, under the assumption that the point-charge model applies,

$$A_6 = -\frac{33}{100}\frac{q_0|e|}{R_0^7}. \quad (7)$$

The quantity γ_J is the Stevens coefficient [36] of the RE ion under consideration and

$$\langle r^6\rangle = \int_0^\infty R_{4f}^2(r)\, r^6\, dr \quad (8)$$

is an average of r^6 over the normalized radial $4f$ wave function $R_{4f}(r)$. The Stevens' operators appearing in Eq. (5) are

$$O_6^0 = 231J_z^6 - 105[3J(J+1) - 7]J_z^4 + [105J^2(J+1)^2 - 525J(J+1) + 294]J_z^2 - 5J^3(J+1)^3 + 40J^2(J+1)^2 - 60J(J+1), \quad (9a)$$

$$O_6^5 = \tfrac{1}{4}[J_z(J_+^5 + J_-^5) + (J_+^5 + J_-^5)J_z]. \quad (9b)$$

Here J_z and $J_\pm = J_x \pm iJ_y$ are the total angular momentum operators. The icosahedral CF energy level scheme is governed by one CF parameter B_6, only, which merely stretches the ladder (or turns it upside down for a negative B_6 value). The CF schemes for the icosahedral crystalline potential have been published for all RE ions [13].

In the case of pentagonal electrostatic potential, the coefficients γ_{20} and γ_{40} in Eq. (3) no longer vanish by symmetry, as they do in the icosahedral case. By transforming into the total angular momentum representation we obtain the pentagonal CF Hamiltonian

$$\mathcal{H}_{\rm CF}^{(5)} = B_2^0O_2^0 + B_4^0O_4^0 + B_6^0O_6^0 + B_6^5O_6^5, \quad (10)$$

where

$$O_2^0 = 3J_z^2 - J(J+1), \quad (11)$$

$$O_4^0 = 35J_z^4 - [30J(J+1) - 25]J_z^2 - 6J(J+1) + 3J^2(J+1)^2, \quad (12)$$

and O_6^0 and O_6^5 are given by Eqs. (9a) and (9b). The coefficients B_n^m show the following dependence on the distance R_j of the jth charge from the RE ion: $B_2^0 \propto R_j^{-3}$, $B_4^0 \propto R_j^{-5}$, and $B_6^0, B_6^5 \propto R_j^{-7}$. When calculating the energy levels of $\mathcal{H}_{\rm CF}^{(5)}$ in the $|J,m\rangle$ basis, the three $B_n^0O_n^0$ terms give diagonal matrix elements, whereas the nonzero matrix elements of $B_6^5O_6^5$ are off-diagonal, so that the matrix has to be diagonalized.

The CF Hamiltonian for the pentagonal charge distribution around the RE ion in Tsai-type i-QCs and approximants is thus given by Eq. (10). It depends on four CF parameters, B_2^0, B_4^0, B_6^0, and B_6^5, and since the conduction electrons make significant contribution to the charge in the metallic state, the point-charge model does not apply. Consequently, no theoretical prediction for the parameters B_n^m can be made.

IV. CF EFFECTS IN THE i-Zn-Ag-Sc-Tm ICOSAHEDRAL QUASICRYSTAL AND THE 1/1 Zn-Sc-Tm APPROXIMANT

A. Samples selection and characterization

Our study of the CF effects on the low-temperature specific heat and magnetic susceptibility has included two pairs of samples, all with the Tsai-type structure. The first pair consisted of icosahedral quasicrystals i-$Zn_{74.5}Ag_{9.5}Sc_{12}Tm_4$ (abbreviated in the following as i-Zn-Ag-Sc-Tm) and i-$Zn_{74.5}Ag_{9.5}Sc_{16}$ (i-Zn-Ag-Sc), whereas the second pair were 1/1 bcc approximants $Zn_{85.5}Sc_{11}Tm_{3.5}$ (1/1 Zn-Sc-Tm) and $Zn_{85.5}Sc_{14.5}$ (1/1 Zn-Sc). The two members of each pair are isostructural, the difference being the population of the (middle) icosahedral shell of the three-shell cluster. In one sample of the pair (termed for convenience the "pure compound"), the icosahedral shell is populated by Sc atoms only, whereas in the complementary sample (the "substituted compound"), a fraction of Sc atoms has been substituted by the RE atom thulium (Tm). The CF effects were studied on the Tm-substituted samples, whereas the samples without Tm

were studied for comparison to demonstrate the effect of the Tm substitution on the physical properties of the pure phase.

The synthesis, formation, x-ray diffraction (XRD) data, and electron microscopy characterization of the i-Zn-Ag-Sc quasicrystal have been reported before [18,37], whereas the description of i-Zn-Fe-Sc-RE (RE = Ho, Er, Tm) quasicrystals, isostructural to our i-Zn-Ag-Sc-Tm, can be found in another publication [25]. It was shown that after a proper annealing process, these i-QCs are thermodynamically stable, forming single phase with P-type (primitive type) icosahedral symmetry $m\bar{3}\bar{5}$. The inner dodecahedron and the outer icosidodecahedron of the three-shell cluster are populated by a mixture of Zn and Ag atoms, whereas the middle icosahedron is populated by Sc atoms in the pure compound and by a mixture of Sc and Tm atoms in the substituted compound. The 1/1 Zn-Sc and 1/1 Zn-Sc-Tm approximants both possess the $Zn_{17}Sc_3$-type structure [29,38]. In both cases, the inner dodecahedron and the outer icosidodecahedron of the three-shell cluster are populated by Zn atoms only, whereas the middle icosahedron is populated by Sc atoms in the pure compound and by a Sc-Tm mixture in the substituted compound.

All four investigated samples were in polygrain morphology. For the i-Zn-Ag-Sc sample preparation, the starting materials were put in an alumina crucible and sealed in a silica tube in an argon atmosphere. After the melting and solidifying operation, the sample was annealed at 746 °C for 20 h and then slowly cooled to room temperature. Its XRD pattern was found identical to that of the i-$Zn_{74.5}Ag_{9.5}Sc_{16}$ published before [37] and is not shown here, whereas the six-dimensional lattice parameter was determined to be $a_{6D} = 0.7146 \pm 0.0001$ nm. The Tm-substituted sample i-Zn-Ag-Sc-Tm was synthesized under similar conditions except for the annealing at 709 °C for 60 h and quenching into water. Its powder XRD pattern, typical of an icosahedral quasicrystal, is shown in Fig. 2(a). Its six-dimensional lattice parameter was determined to be $a_{6D} = 0.7183 \pm 0.0001$ nm, very close to that of the pure sample. The 1/1 Zn-Sc sample was annealed at 455 °C for 50 h and then slowly cooled to room temperature. Its powder XRD pattern, typical of a 1/1 Tsai-type approximant, is shown in Fig. 2(b) and its bcc lattice parameter was determined to be $a = 1.3852 \pm 0.0001$ nm. The Tm-substituted sample 1/1 Zn-Sc-Tm was annealed at 611 °C for 80 h and then quenched into water. Its powder XRD pattern is shown in Fig. 2(c) and its bcc lattice parameter was $a = 1.3903 \pm 0.0001$ nm. Further details of the samples synthesis and characterization of the substituted compounds i-Zn-Ag-Sc-Tm and 1/1 Zn-Sc-Tm will be published elsewhere. The XRD patterns of all four investigated samples show sharp diffraction peaks, where most of the peaks could be indexed to a single phase, revealing good structural order. The six-dimensional lattice parameters of the two i-QC samples are very close to each other, and the same holds for the bcc lattice parameters of the two approximants, indicating that in both cases the structures of the pure and the Tm-substituted samples are the same and the small lattice expansion of the Tm-substituted samples is due to a slightly larger atomic radius of Tm (0.1746 nm), as compared to Sc (0.1641 nm) [39]. The partial (random) Tm-for-Sc substitution on the middle icosahedron of the three-shell cluster is thus the only significant structural difference between the pure and the substituted compounds.

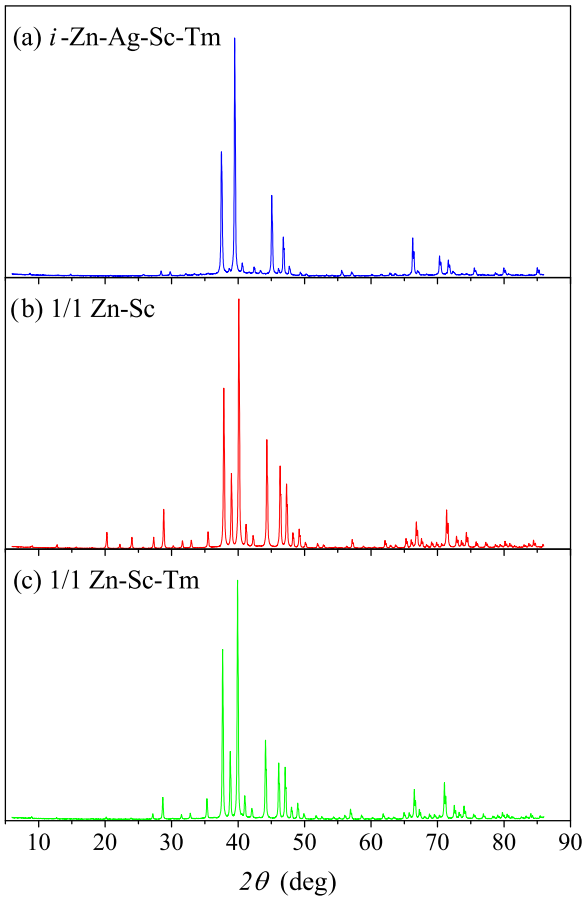

FIG. 2. Powder XRD patterns of (a) i-Zn-Ag-Sc-Tm icosahedral quasicrystal, (b) 1/1 Zn-Sc approximant, and (c) 1/1 Zn-Sc-Tm approximant measured using Cu $K\alpha$ radiation in a step scan mode at steps of 0.01°.

Temperature-dependent electrical resistivity ρ is another convenient quantity to characterize metallic samples. We have measured the resistivity of all four investigated samples, but since ρ is insensitive to the CF effects, we present the results in the Supplemental Material (Fig. S1) [40].

B. Experiment

The measurements of the specific heat and the electrical resistivity were conducted by a Quantum Design Physical Property Measurement System PPMS 9T, equipped with a 9 T magnet and operating in the temperature range between 400 and 0.35 K. Low temperatures below 2 K were reached by a ^{3}He cryostat. Magnetic measurements were conducted by a Quantum Design MPMS XL-5 SQUID magnetometer equipped with a 5 T magnet and operating in the temperature range 400–1.9 K.

C. Magnetic susceptibility

The magnetism of the Tm-containing i-Zn-Ag-Sc-Tm icosahedral quasicrystal and its 1/1 Zn-Sc-Tm approximant is originating from the thulium ions since the triply ionized Sc^{3+}

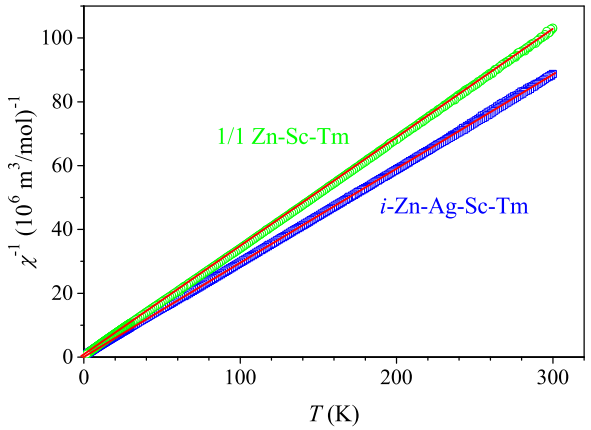

FIG. 3. Temperature-dependent magnetic susceptibility of the *i*-Zn-Ag-Sc-Tm quasicrystal and the 1/1 Zn-Sc-Tm approximant in a χ^{-1} versus T plot. The fits with Eq. (13) are shown by solid lines (red online).

ions possess the electronic configuration of the noble gas argon with no unpaired electrons and are hence diamagnetic. The magnetic susceptibility χ of the *i*-Zn-Ag-Sc pure quasicrystal was studied before and was indeed reported to be negative diamagnetic [37].

The magnetic susceptibility $\chi = M/H$ of the *i*-Zn-Ag-Sc-Tm and the 1/1 Zn-Sc-Tm was studied in the temperature range 1.9–300 K in a magnetic field of $\mu_0 H = 10\,\text{mT}$. The analysis was performed by assuming validity of the Curie-Weiss law,

$$\chi = \frac{C_{\text{CW}}}{T - \theta_{\text{CW}}}, \tag{13}$$

where C_{CW} is the Curie-Weiss constant and θ_{CW} is the Curie-Weiss temperature. There can be an additional temperature-independent term χ_0 added to the right side of Eq. (13), accounting for the Larmor diamagnetic contribution χ_{dia} due to the atomic cores and the two contributions from the conduction electrons—the Landau diamagnetic contribution χ_L due to the electron orbital circulation and the Pauli spin paramagnetic contribution χ_P. The Larmor susceptibility was calculated from literature tables to amount $\chi_{\text{dia}} = -1.4 \times 10^{-11}\,\text{m}^3/\text{mol}$ for the *i*-Zn-Ag-Sc-Tm and $\chi_{\text{dia}} = -1.2 \times 10^{-11}\,\text{m}^3/\text{mol}$ for the 1/1 Zn-Sc-Tm. The Landau and Pauli contributions are of the same (absolute) order of magnitude as χ_{dia}, so that the constant term χ_0 is by several orders of magnitude smaller than the Curie-Weiss susceptibility of the Tm atoms at low temperatures. For that reason χ_0 was omitted from Eq. (13).

The temperature-dependent magnetic susceptibility data are shown in Fig. 3 in a χ^{-1} versus T plot. The fits with Eq. (13) (solid lines) yielded the following parameter values for the *i*-Zn-Ag-Sc-Tm: $C_{\text{CW}} = (3.3 \pm 0.2) \times 10^{-6}\,\text{m}^3\text{K/mol}$ [or $C_{\text{CW}} = (8.2 \pm 0.5) \times 10^{-5}\,\text{m}^3\text{K/mol Tm}$, when recalculated per mole of Tm] and $\theta_{\text{CW}} = -0.9 \pm 1.0\,\text{K}$. For the 1/1 Zn-Sc-Tm, the fit parameters are $C_{\text{CW}} = (2.9 \pm 0.2) \times 10^{-6}\,\text{m}^3\text{K/mol}$ [or $C_{\text{CW}} = (8.4 \pm 0.5) \times 10^{-5}\,\text{m}^3\text{K/mol Tm}$] and $\theta_{\text{CW}} = -0.7 \pm 1.0\,\text{K}$.

The Curie-Weiss constant C_{CW} was used to determine the mean effective magnetic moment $\bar{\mu}_{\text{eff}} = \bar{p}_{\text{eff}}\mu_B$ per Tm ion. Here $\bar{p}_{\text{eff}}$ is the mean effective Bohr magneton number that can be calculated using the formula [41] $\bar{p}_{\text{eff}} = \sqrt{3C_{\text{CW}}k_B/(N_A\mu_B^2\mu_0)}$ (where N_A is the Avogadro number and C_{CW} is given in units per mole of Tm atoms). For the *i*-Zn-Ag-Sc-Tm we obtained $\bar{p}_{\text{eff}} = 7.2 \pm 0.2$, whereas for the 1/1 Zn-Sc-Tm it amounts to $\bar{p}_{\text{eff}} = 7.3 \pm 0.2$. These values are within the experimental uncertainty the same as the measured Bohr magneton number of a bare Tm^{3+} ion ($p = 7.3$), demonstrating that the Tm magnetic moments in the *i*-Zn-Ag-Sc-Tm and the 1/1 Zn-Sc-Tm phases assume their full free-ion values of $7.3\,\mu_B$.

The Curie-Weiss temperature is an indication of either the spin-spin exchange coupling or the CF effects (recall that an effective Curie-Weiss behavior of the susceptibility is observed for a nonmagnetic CF ground state). The fit-determined values of θ_{CW} from the data in the entire investigated temperature range 1.9–300 K for both the *i*-Zn-Ag-Sc-Tm and the 1/1 Zn-Sc-Tm are within the experimental uncertainty equal to zero, so that the temperature-dependent magnetic susceptibility in fact obeys the Curie law $\chi = C_{\text{CW}}/T$, pertinent to an ensemble of paramagnetic free (uncoupled) ions, rather than the Curie-Weiss law. The small nonzero θ_{CW} values ($\theta_{\text{CW}} = -0.9 \pm 1.0\,\text{K}$ for the *i*-Zn-Ag-Sc-Tm and $\theta_{\text{CW}} = -0.7 \pm 1.0\,\text{K}$ for the 1/1 Zn-Sc-Tm), where the experimental uncertainty is larger than the mean value, should be considered merely as an additional fit parameter in Eq. (13), which slightly improves the fits, but not as an indication of a weak antiferromagnetic-type exchange coupling between the Tm moments or the CF effects. There is no Curie-Weiss deviation of the magnetic susceptibility from the Curie behavior of free Tm^{3+} ions down to the lowest investigated temperature of 1.9 K. Here it is important to recall that the absence of the CF-induced Curie-Weiss behavior of the susceptibility does not mean the absence of CF effects, but merely excludes a nonmagnetic CF-split ground state. The *i*-Zn-Ag-Sc-Tm and 1/1 Zn-Sc-Tm samples can be thus to a good approximation classified as Curie paramagnets (at least down to the lowest investigated temperature of 1.9 K), where the Tm^{3+} moments assume their full free-ion values of $7.3\,\mu_B$.

Since the magnetic moments of the Tm^{3+} ions are sizable, it is instructive to estimate the strength of the magnetic dipole-dipole interaction between the nearest-neighbor Tm moments on the icosahedral shell. For a qualitative estimate we take the nearest-neighbor Tm-Tm distance to be $r = 0.57\,\text{nm}$ (the value determined for the Ce-Ce distance in the 1/1 $Ce_{15}Au_{65}Sn_{20}$ bcc approximant). The order of magnitude of the dipole-dipole energy is then obtained as $E_{dd}/k_B \approx (\mu_0/4\pi)(\bar{p}_{\text{eff}}\mu_B)^2/r^3k_B = 0.18\,\text{K}$.

D. Specific heat

Specific heat is a crucial quantity to observe the Schottky effect. The low-temperature specific heat of a RE-containing metallic alloy in the paramagnetic phase can be written as a sum of the electronic, lattice, and Schottky contributions [42]

$$C = \gamma T + \beta_3 T^3 + C_{\text{Sch}}. \tag{14}$$

Here γ is the electronic specific heat coefficient that is related to the electronic density of states (DOS) $g(\varepsilon_F)$ at the Fermi energy ε_F via the relation $\gamma = (\pi^2/3)k_B^2 g(\varepsilon_F)$, whereas β_3 is the lattice specific heat coefficient, which is

within the Debye model related to the Debye temperature via the expression $\theta_D = (12\pi^4 R/5\beta_3)^{1/3}$ and R is the gas constant. The Schottky specific heat, introduced by the RE ions that occupy a set of discrete energy levels $\Delta_i = \varepsilon_i/k_B$ (in temperature units), is written as [42]

$$C_{\mathrm{Sch}} = \frac{R}{T^2}\frac{\sum_{i,j}\left(\Delta_i^2 - \Delta_i\Delta_j\right)\exp[-(\Delta_i+\Delta_j)/T]}{\sum_{i,j}\exp[-(\Delta_i+\Delta_j)/T]}, \quad (15)$$

where

$$Z = \sum_i \exp(-\Delta_i/T) \quad (16)$$

is the partition function and i runs over all the levels. In Eq. (15), C_{Sch} is written per one mole of RE atoms, whereas in the case that the RE molar fraction in the substance is x, the right side should be multiplied by x (i.e., a transformation $R \to xR$ should be made). The temperature variation of C_{Sch} as given by Eq. (15) can be understood by considering that the specific heat measures the change of internal energy of the system with temperature due to thermal excitations between its energy levels. In the $T \to 0$ limit, the ground state is populated only and hence the transition probability between levels is negligible, so that $C_{\mathrm{Sch}} \to 0$ as $T \to 0$. At high enough temperatures (for T much larger than the energy differences between the levels), all levels are almost equally populated and the transitions between the states do not change their populations significantly anymore, so that $C_{\mathrm{Sch}} \to 0$ as $T \to \infty$. Only when T is on the scale of the energy differences $\Delta_i - \Delta_j$, the transitions between the levels alter their populations to an appreciable degree, leading to a large C_{Sch} contribution that exhibits a broad maximum at a temperature of a fraction of $\Delta_i - \Delta_j$. To illustrate, for a two-level system with the separation $\delta = \Delta_2 - \Delta_1$, the low- and high-temperature limits of Eq. (15) are

$$C_{\mathrm{Sch}} \approx R\left(\frac{\delta}{T}\right)^2 \exp(-\delta/T), \quad T \ll \delta, \quad (17a)$$

$$C_{\mathrm{Sch}} \approx R\left(\frac{\delta}{2T}\right)^2, \quad T \gg \delta, \quad (17b)$$

and the C_{Sch} maximum appears at a temperature $T_m \approx 0.42\,\delta$.

The energies ε_i of the set of discrete levels are calculated from the RE-ion Hamiltonian, which contains the CF term and the interaction between the ionic moment and the magnetic field at the site of the ion that is a sum of the external field B and the dipolar field B_{dip}. The Hamiltonian may also contain the Heisenberg exchange term, but since the analysis of the magnetic susceptibilities of i-Zn-Ag-Sc-Tm and 1/1 Zn-Sc-Tm has yielded zero Curie-Weiss temperatures (a measure of the exchange interaction strength), the exchange term will be omitted. The dipolar field B_{dip} due to the Tm-Tm dipolar interaction can also be neglected due to the relatively large spatial separation between the Tm neighbors in the crystal structure (according to the previously estimated magnitude of the dipole-dipole energy, the peak in C_{Sch} due to the dipole interaction in zero external magnetic field could occur at temperatures below 100 mK). Writing the RE-ion moment as $\vec{\mu} = -g_J\,\mu_B\,\vec{J}$, where g_J is the Landé g factor ($g_J = 1.17$ for the Tm^{3+} ions in the Hund's ground state $^3H_6$ with $L = 5$, $S = 1$, $J = 6$), the total Hamiltonian is

$$\mathcal{H} = g_J\mu_B B J_{z'} + \mathcal{H}_{\mathrm{CF}}. \quad (18)$$

The CF Hamiltonian is to a good approximation given by Eq. (10), which is written in the crystal-fixed coordinate system (x,y,z) as defined in Fig. 1(d) (the z axis points along one of the fivefold axes of the three-shell cluster). The Zeeman term is, on the other hand, written in the laboratory system (x',y',z'), where the z' axis points along the direction of the external magnetic field.

The $\mathcal{H}_{\mathrm{CF}}^{(5)}$ Hamiltonian is parametrized by four CF parameters, which experimentally cannot be extracted reliably from fits of the specific heat. Since $B_2^0 O_2^0$ is the leading term in the pentagonal CF Hamiltonian, we shall perform in the following an approximate analysis of the low-temperature specific heat data by keeping this term only, so that the energy-level scheme of the Tm^{3+} ions will be calculated for the Hamiltonian

$$\mathcal{H} = g_J\mu_B B J_{z'} + B_2^0\left[3J_z^2 - J(J+1)\right]. \quad (19)$$

In the absence of an external magnetic field ($B = 0$), the energy levels are determined by the matrix elements of the CF term, yielding $\varepsilon_m = B_2^0[3m^2 - J(J+1)]$ with $m = -6, -5, \ldots, 5, 6$. Except for ε_0, all other levels show $\pm m$ degeneracy, so that the energy level scheme is composed of a nondegenerate level ε_0 and six doubly degenerate levels $\varepsilon_{\pm m}$ with $m = 1, \ldots, 6$, which are unequally spaced [Fig. 4(a)].

When computing the energy levels in the presence of a magnetic field, we need to take into account the fact that the quantization axis z' of the Zeeman Hamiltonian generally differs from the quantization axis z of the CF Hamiltonian. Analytical solutions can be obtained in the limits when the Zeeman interaction is either weak or strong as compared to the CF interaction. We consider first the case of a weak magnetic field, where the Zeeman term is a perturbation to the CF term. In this case, the moments are quantized along the z direction. Defining x' axis to lie in the plane containing z' and z, and the angle between z' and z is α, we have

$$J_{z'} = J_z\cos\alpha - J_x\sin\alpha. \quad (20)$$

Inserting Eq. (20) into Eq. (19), we obtain the energy levels in first-order perturbation

$$\varepsilon_m = g_J\mu_B Bm\cos\alpha + B_2^0[3m^2 - J(J+1)]. \quad (21)$$

The $\pm m$ energy levels, which are doubly degenerate in the absence of a magnetic field, are now split by the Zeeman energy $2g_J\mu_B Bm\cos\alpha$, so that the energy level scheme contains the ε_0 level plus six Zeeman-split CF doublets, 13 nondegenerate levels altogether [Fig. 4(b)].

In a strong magnetic field, the CF term is a perturbation to the Zeeman term, so that the moments are quantized along the z' direction. Using the transformation

$$J_z = J_{z'}\cos\alpha + J_{x'}\sin\alpha, \quad (22)$$

and inserting it into Eq. (20), we obtain diagonal terms $J_{z'}$ and $J_{z'}^2$ and also terms $J_{x'}^2$ and $J_{z'}J_{x'} + J_{x'}J_{z'}$. Since $J_{x'}$ has vanishing diagonal elements, the terms involving this operator do not contribute in first order. The $J_{x'}^2$ operator has diagonal elements, which are evaluated as

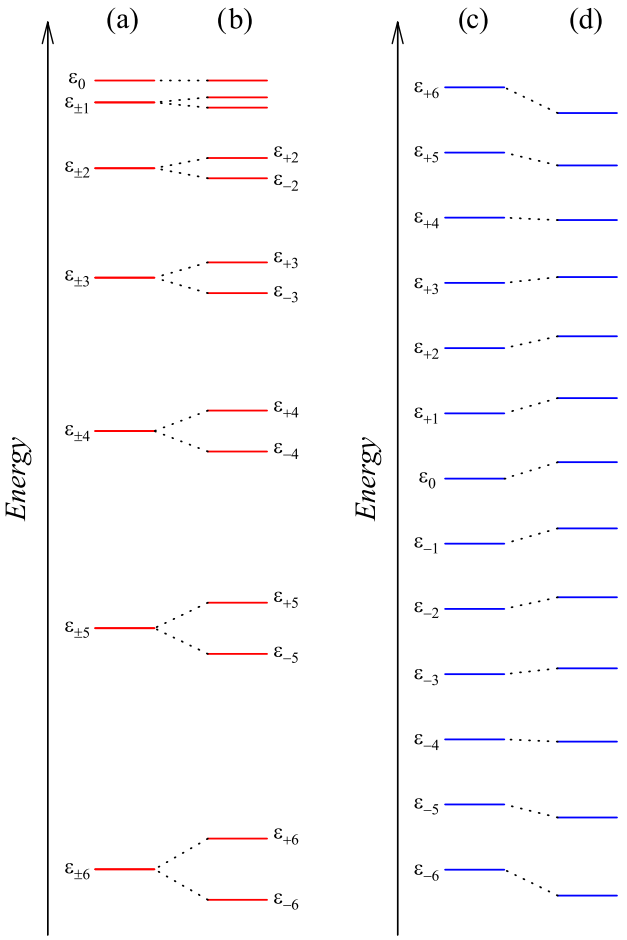

FIG. 4. Energy-level scheme of Tm^{3+} ions according to the Hamiltonian of Eq. (19): (a) Pure CF energy levels in zero external magnetic field ($B = 0$), assuming $B_2^0 < 0$; (b) Zeeman-split CF energy levels in the weak-field limit according to Eq. (21) for the ratio $g_J\mu_B B/|B_2^0| = 0.7$. (c) Pure Zeeman energy levels and (d) CF-perturbed Zeeman levels in the strong-field limit according to Eq. (23). $B_2^0 < 0$ is assumed again and the ratio of the interactions strengths was taken as $|B_2^0|/g_J\mu_B B = 0.006$. In (a) and (b) the vertical axis shows the normalized energy $\varepsilon_m/|B_2^0|$, whereas in (c) and (d), $\varepsilon_m/g_J\mu_B B$ is given. The case $\cos\alpha = 1$ is assumed in Eqs. (21) and (23).

$\langle m|J_{x'}^2|m\rangle = (1/2)[J(J+1) - m^2]$. By collecting terms, we find in first-order perturbation

$$\varepsilon_m = g_J\mu_B Bm + B_2^0\left(\frac{3\cos^2\alpha - 1}{2}\right)[3m^2 - J(J+1)]. \tag{23}$$

The 13 equidistantly spaced pure Zeeman levels [Fig. 4(c)] become shifted by the CF interaction, where the ε_m and ε_{-m} CF-perturbed Zeeman levels are shifted by the same amount [Fig. 4(d)]. In the intermediate regime of comparable Zeeman and CF interactions, no simple analytical solution can be obtained and the energy levels are computed by diagonalizing the Hamiltonian of Eq. (19).

The energy levels of a Tm^{3+} ion given by Eqs. (21) and (23) depend on the orientation of the fivefold axis of the three-shell cluster with respect to the magnetic field direction via the $\cos\alpha$ function. Since Tm atoms substitute randomly Sc atoms on the icosahedral shell, many different orientations are realized throughout the *i*-Zn-Ag-Sc-Tm and 1/1 Zn-Sc-Tm structures. In addition, our investigated samples were in a polygrain morphology with randomly oriented grains, so that different values of $u = \cos\alpha$ are equally probable on the interval $u \in [1, -1]$ with the probability density $g(u) = 1/2$. Performing the powder average, we sum the Schottky specific heat contributions over all Tm^{3+} ions to obtain

$$C_{\rm Sch}^p = \int_{-1}^{1} C_{\rm Sch}(u)\ \ g(u)du = \frac{R}{2T^2}\int_{-1}^{1} du \times \frac{\sum_{i,j}[\Delta_i(u)^2 - \Delta_i(u)\Delta_j(u)]\exp\{-[\Delta_i(u)+\Delta_j(u)]/T\}}{\sum_{i,j}\exp\{-[\Delta_i(u)+\Delta_j(u)]/T\}}, \tag{24}$$

where the superscript p stands for "powder" and $\Delta_i(u) = \varepsilon_i(u)/k_B$ are given by Eqs. (21) and (23).

In RE-containing solids, the Schottky specific heat contains another term that additionally aggravates the analysis in the $T \to 0$ limit. This is the nuclear Schottky effect, which shows up at very low temperatures, but can readily be observed experimentally. The nuclear Schottky effect is treated in the Appendix.

1. *Low-temperature specific heat of the 1/1 Zn-Sc-Tm and 1/1 Zn-Sc approximants*

We present first the specific heat of the 1/1 Zn-Sc and the 1/1 Zn-Sc-Tm approximants. The low-temperature data in zero magnetic field are shown in Fig. 5(a) in a C versus T plot. The specific heat of the 1/1 Zn-Sc-Tm substituted compound exhibits a broad peak at the temperature of about 1.0 K, whereas the specific heat of the 1/1 Zn-Sc pure compound is much smaller and does not exhibit any such feature. A broad peak in the specific heat at low temperatures is found in some magnetic systems with exchange-coupled spins like in spin glasses [43] where it originates from thermal excitations of the collective spin state (spin reorientations), but the peak can also be the Schottky specific heat contribution. For the 1/1 Zn-Sc-Tm, magnetic origin of the specific heat maximum can be excluded, because the Curie-Weiss temperature of the magnetic susceptibility was found zero and the susceptibility shown in Fig. 3 is of a Curie type, demonstrating that the Tm^{3+} moments can be treated as uncoupled. The specific heat maximum is thus a single-ion property, which is straightforward to associate with the Schottky specific heat. The specific heat of the two compounds in the entire investigated temperature range up to 300 K is shown in the inset of Fig. 5(a). The 1/1 Zn-Sc pure compound shows a sharp anomaly at $T_c = 163$ K, appearing at the order-disorder phase transition associated with freezing of the central Zn_4 tetrahedron reorientations, whereas no such transition is observed for the 1/1 Zn-Sc-Tm substituted compound.

The low-temperature specific heat of the 1/1 Zn-Sc pure compound is analyzed in the inset of Fig. 5(b), where the data are presented in a C/T versus T^2 plot. For a regular metallic alloy without the Schottky contribution ($C_{\rm Sch} = 0$), Eq. (14) yields $C/T = \gamma + \beta_3 T^2$, and the data fall on a straight line in this kind of a plot. The electronic specific heat

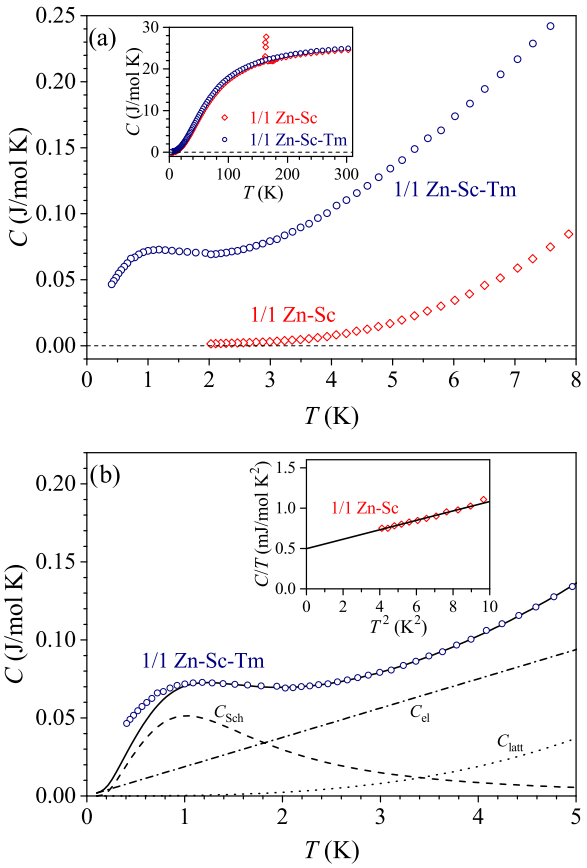

FIG. 5. (a) Low-temperature specific heat of the 1/1 Zn-Sc and 1/1 Zn-Sc-Tm approximants in zero magnetic field. The inset shows the specific heats in the temperature range up to 300 K. (b) Analysis of the low-temperature zero-field specific heat of the 1/1 Zn-Sc-Tm substituted approximant by Eq. (14), using Eq. (15) for the Schottky contribution (solid curve). The three contributions to the total specific heat (the Schottky term $C_{\rm Sch}$, the electronic term $C_{\rm el} = \gamma T$, and the lattice term $C_{\rm latt} = \beta_3 T^3$) are also shown separately. The inset shows the low-temperature specific heat of the 1/1 Zn-Sc pure approximant in a C/T versus T^2 plot. Solid line is the fit with $C/T = \gamma + \beta_3 T^2$.

coefficient γ and the lattice coefficient β_3 are then obtained from the intercept of the vertical axis and the slope of the line, respectively. The data of the 1/1 Zn-Sc indeed fall on a straight line, confirming its regular metallic character, and the analysis (solid line) has yielded $\gamma = 0.50\,\mathrm{mJ/mol\,K^2}$ and $\beta_3 = 5.8 \times 10^{-2}\,\mathrm{mJ/mol\,K^4}$, wherefrom the Debye temperature $\theta_D = 322\,\mathrm{K}$ is obtained.

The low-temperature specific heat of the 1/1 Zn-Sc-Tm substituted compound is analyzed in the main panel of Fig. 5(b) in a C versus T scale. The total specific heat C was reproduced theoretically by Eq. (14), using Eq. (15) for the Schottky contribution. The Hamiltonian of Eq. (19) by putting the magnetic field $B = 0$ was taken for the calculation of the energy levels of the Tm^{3+} ions, so that only the CF term described by the parameter B_2^0 remained and the energy level scheme of Fig. 4(a) applies. The powder average of the Schottky contribution was performed via Eq. (24). The theoretical curve [solid curve in Fig. 5(b)] was obtained by the set of fit parameters $B_2^0/k_B = -(4.4 \pm 0.1) \times 10^{-2}\,\mathrm{K}$, $\gamma = 21 \pm 4\,\mathrm{mJ/mol\,K^2}$, and $\beta_3 = 0.30 \pm 0.03\,\mathrm{mJ/mol\,K^4}$ (yielding $\theta_D = 187 \pm 6\,\mathrm{K}$). The three contributions to the total specific heat (the Schottky term $C_{\rm Sch}$, the electronic term $C_{\rm el} = \gamma T$, and the lattice term $C_{\rm latt} = \beta_3 T^3$) are also shown separately in Fig. 5(b). $C_{\rm Sch}$ exhibits a peak at 1.0 K and its "high-temperature" decaying tail extends up to about 5 K. $C_{\rm el}$ grows linearly with the temperature (starting from zero at $T = 0$), whereas $C_{\rm latt}$ contributes almost negligibly to the total specific heat in the temperature region where $C_{\rm Sch}$ is large. Around the $C_{\rm Sch}$ maximum, the Schottky contribution prevails over the sum $C_{\rm el} + C_{\rm latt}$, accounting for about 70% of the total specific heat at 1.0 K. Due to the dominance of $C_{\rm Sch}$, the fit-determined values of the γ and β_3 coefficients are uncertain and should be considered as indicative only, as their values can change significantly in a fit procedure already by a small change of the Schottky contribution. The theoretical total specific heat curve reproduces well the experimental data in the fitted temperature range up to 5 K, except below the $C_{\rm Sch}$ maximum (below 1.0 K), where the theoretical curve decays faster than the experimental data. Reasons for this discrepancy can be numerous (the approximate analysis by using the leading term $B_2^0 O_2^0$ of the CF Hamiltonian only, the neglect of the dipolar magnetic field $B_{\rm dip}$, and other approximations used to derive an analytical form of the CF Hamiltonian for the $C_{\rm Sch}$ calculation).

In order to obtain trustworthy values of the γ and β_3 coefficients, one might consider to isolate the Schottky specific heat term from the experimental data by subtracting the total low-temperature specific heat of the 1/1 Zn-Sc pure compound from the specific heat of the 1/1 Zn-Sc-Tm substituted compound. This technique would yield a valid result in the case that the γ and β_3 coefficients would not be changed significantly by the partial Tm-for-Sc substitution. A comparison of the specific heats of the pure and substituted compounds in Fig. 5(a) shows that this is not the case, as the introduction of 3.5 at. % of Tm has obviously changed the γ and β_3 quite drastically.

In the next step, the specific heat of the 1/1 Zn-Sc-Tm was measured in a magnetic field at the following field values: $B = 0, 0.1, 0.2, 0.3, 0.4, 0.5, 0.6, 0.7, 0.8, 0.9, 1, 1.3, 2, 3, 4, 5, 6, 7, 8$, and 9 T. The low-temperature data in the temperature interval between 0.4 and 2.0 K are shown in Fig. 6(a). For clarity of presentation, the data for a selected set of field value are only shown in the graph. We observe that the maximum of $C_{\rm Sch}$ is shifting to higher temperatures with increasing field and for fields larger than 1.0 T, the maximum has already moved outside of the presented temperature interval, so that only the low-temperature increasing part of $C_{\rm Sch}$ remains to be observed. The specific heat in zero field and in a 9 T field in a larger temperature interval up to 10 K is shown in the inset of Fig. 6(a). The 9-T specific heat is smaller than the zero-field specific heat between 0.4 and about 6 K, but crosses it and becomes larger at temperatures above 6.5 K as the $C_{\rm Sch}$ maximum has shifted to higher temperatures in the field.

The total specific heat C in a magnetic field was reproduced theoretically using the theory presented in the preceding section, by just including the Zeeman term into the Hamiltonian of Eq. (19), whereas the values of the parameters B_2^0, γ, and β_3 were taken from those determined from the fit of the zero-field specific heat [given by the solid curve in Fig. 5(b)]. Inspecting the relative magnitudes of the CF and the Zeeman

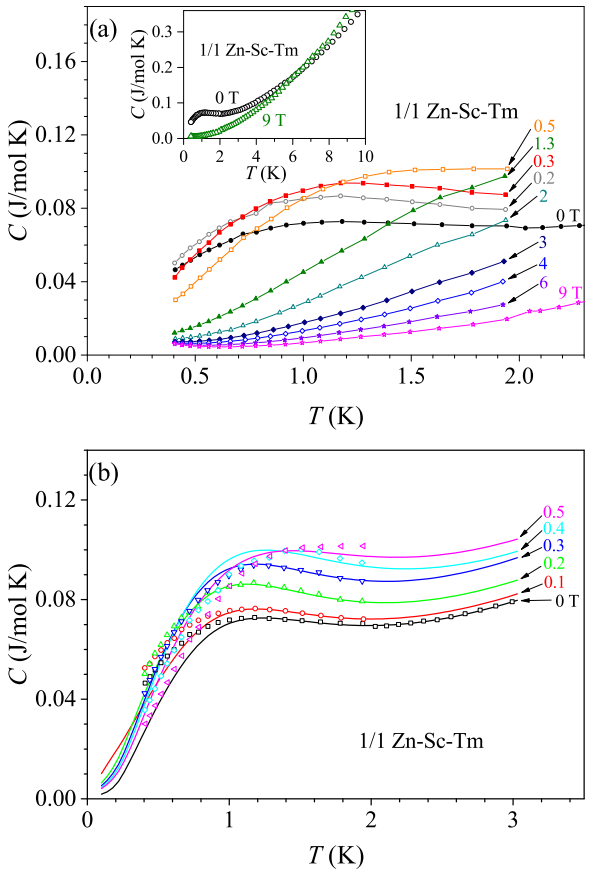

FIG. 6. (a) Low-temperature specific heat of the 1/1 Zn-Sc-Tm approximant in a magnetic field for a selected set of field values (indicated on the graph). The inset shows the specific heat in zero field and in a 9 T field in a larger temperature interval up to 10 K. (b) Specific heat in the low-field region at $B = 0, 0.1, 0.2, 0.3, 0.4$, and 0.5 T. Theoretical fits (solid curves) were obtained by the analytical model, where the Zeeman interaction is a perturbation of the CF term as expressed by Eq. (21).

terms in the Hamiltonian of Eq. (19), we find that the CF energy-level splittings $(\varepsilon_{m+1} - \varepsilon_m)/k_B = (3B_2^0/k_B)(2m+1)$ amount to $|\varepsilon_6 - \varepsilon_5|/k_B = 1.45\,\mathrm{K}$, $|\varepsilon_5 - \varepsilon_4|/k_B = 1.19\,\mathrm{K}$, $|\varepsilon_4 - \varepsilon_3|/k_B = 0.92\,\mathrm{K}$, ... The Zeeman splitting between the adjacent levels is $(\varepsilon_{m+1} - \varepsilon_m)/k_B = g_J\mu_B B/k_B = 0.79B[\mathrm{T}]$ K (where B is inserted in Tesla units), which amounts to 0.08 K in 0.1 T field, 0.4 K in 0.5 T, 0.8 K in 1 T, and 7.1 K in a 9 T field. These values suggest that the analytical perturbative treatment of the magnetic-field influence on the specific heat, where the Zeeman interaction is a small perturbation of the CF term as expressed by Eq. (21) [and the energy level scheme of Fig. 4(b) applies] is justified in the low-field regime of our experiments up to about 0.5 T. Theoretical fits of the specific heat in the low-field region for $B = 0$, 0.1, 0.2, 0.3, 0.4, and 0.5 T are shown in Fig. 6(b). We observe that the Schottky peak moves with increasing field to higher temperatures and the energy-level scheme shown in Fig. 4(b) [calculated from Eq. (21)] reproduces reasonably well the experimental data. For higher magnetic fields, the Zeeman and the CF terms become comparable, so that the weak-field analytical perturbative treatment is no longer adequate. The strong-field perturbative treatment as given by Eq. (23) may in principle become adequate in the high-field limit of our experiments (recall that in a 9 T field, the Zeeman splitting amounts to 7.1 K, as compared to the CF splittings of about 1 K), but the Schottky peak in the high field has already moved to temperatures where the low-temperature cubic approximation of the lattice specific heat $C_{\mathrm{latt}} = \beta_3 T^3$ may no longer be satisfactory (usually a $\beta_5 T^5$ correction needs to be added at higher temperatures, which introduces an additional fit parameter), so we skip that analysis.

In addition to the ionic Schottky specific heat C_{Sch} just described, the total specific heat of the 1/1 Zn-Sc-Tm also contains the nuclear Schottky term C_{Sch}^n due to the discrete energy levels of the ^{169}Tm nuclei in a large effective magnetic field B_{eff} arising from the orbiting $4f$ electrons (see the Appendix). The Zeeman splitting of the ^{169}Tm nuclear levels in a magnetic field B is $\delta_n = \gamma_n \hbar B/k_B$. The nuclear gyromagnetic ratio γ_n can be calculated from NMR frequency tables ($\gamma_n = 2\pi\nu_0/B$, where ν_0 is the nuclear Larmor frequency in a field B), yielding for the ^{169}Tm isotope $\delta_n = 1.7 \times 10^{-5}\, B[\mathrm{T}]$ K. For the laboratory field of, e.g., 9 T, $\delta_n = 1.5$ mK is negligibly small, but for the effective field B_{eff} of several 100 T it becomes significant. For the investigated 1/1 Zn-Sc-Tm, the precise value of B_{eff} is not known, but for the lanthanide series, B_{eff} can generally be well in excess of 300 T. For a 300 T field, $\delta_n = 85$ mK, so that a part of the "high-temperature" decaying tail $C_{\mathrm{Sch}}^n \propto T^{-2}$ might be observed experimentally as a low-temperature upturn in the total specific heat on our accessible temperature scale down to 0.4 K. For the 1/1 Zn-Sc-Tm, the low-temperature upturn in the total specific heat due to the nuclear Schottky contribution is best observed in the specific heat data taken in external magnetic fields larger than 5 T, because the ionic Schottky peak at such fields has already moved away from the $T \to 0$ region, so that the effect of the much smaller nuclear contribution becomes readily observed. The low-temperature experimental total specific heat in magnetic fields 6, 7, 8, and 9 T is shown on an expanded scale in Fig. 7(a), where the T^{-2}-type upturn in the $T \to 0$ limit is clearly observed. The nuclear Schottky upturn is a small effect, which can usually be neglected, but it is important in cases when the electronic properties in the $T \to 0$ limit are derived from the specific heat, as both the ionic and the nuclear Schottky effects can be mistakenly interpreted as an electronic effect due to interacting electrons, as will be discussed in Sec. V.

2. *Low-temperature specific heat of the i-Zn-Ag-Sc-Tm and i-Zn-Ag-Sc quasicrystals*

The low-temperature specific heat was investigated also for the *i*-Zn-Ag-Sc-Tm and *i*-Zn-Ag-Sc pair of icosahedral quasicrystals by performing the same set of experiments and analysis steps as for the pair of the approximants. The results are qualitatively similar to those for the approximants, with some quantitative differences. The low-temperature data in zero magnetic field are shown in Fig. 8(a) in a C versus T plot. The specific heat of the *i*-Zn-Ag-Sc-Tm substituted compound exhibits a Schottky contribution with the peak at about 0.8 K, whereas the specific heat of the *i*-Zn-Ag-Sc pure compound is much smaller and does not exhibit any anomaly. The specific heats up to 300 K are shown in the inset of Fig. 8(a). Neither

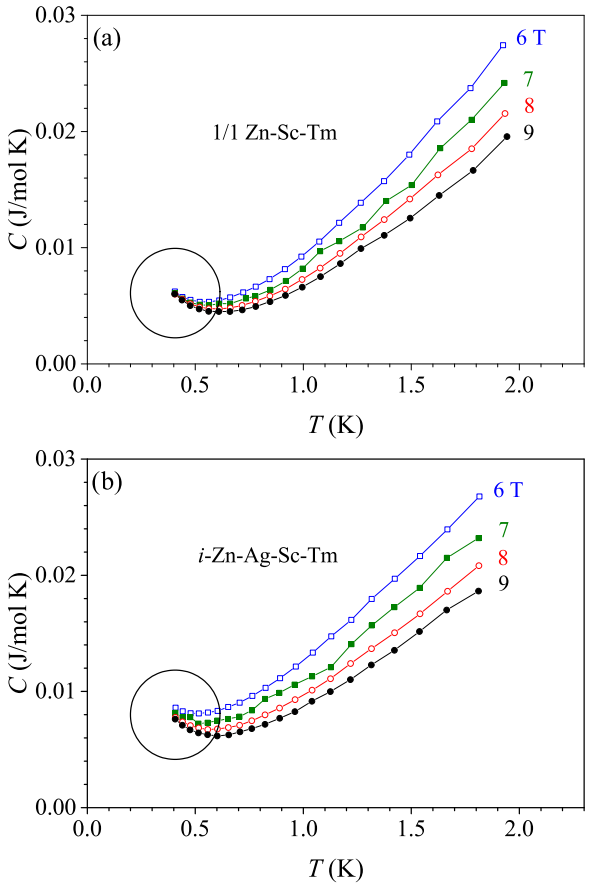

FIG. 7. Low-temperature specific heat of (a) 1/1 Zn-Sc-Tm approximant and (b) i-Zn-Ag-Sc-Tm quasicrystal in magnetic fields between 6 and 9 T, showing the T^{-2}-type upturn in the $T \to 0$ limit due to the nuclear Schottky contribution (encircled on the graphs).

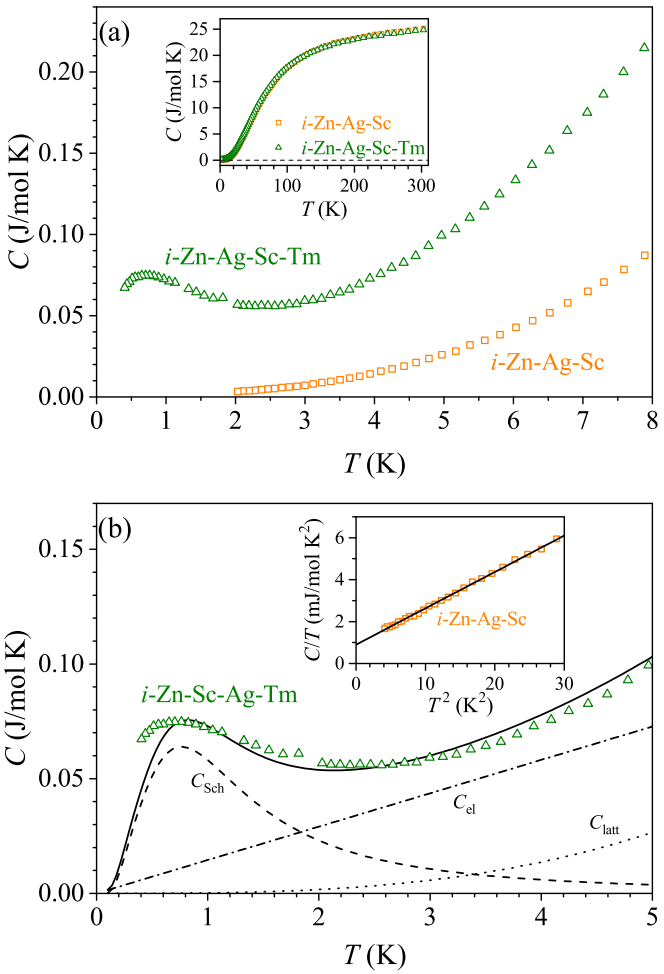

FIG. 8. (a) Low-temperature specific heat of the i-Zn-Ag-Sc and i-Zn-Ag-Sc-Tm quasicrystals in zero magnetic field. The inset shows the specific heats in the temperature range up to 300 K (the curves are indistinguishable on the graphs). (b) Analysis of the low-temperature zero-field specific heat of the i-Zn-Ag-Sc-Tm substituted quasicrystal by Eq. (14), using Eq. (15) for the Schottky contribution (solid curve). The three contributions to the total specific heat (the Schottky term $C_{\rm Sch}$, the electronic term $C_{\rm el} = \gamma T$, and the lattice term $C_{\rm latt} = \beta_3 T^3$) are also shown separately. The inset shows the low-temperature specific heat of the i-Zn-Ag-Sc pure quasicrystal in a C/T versus T^2 plot. Solid line is the fit with $C/T = \gamma + \beta_3 T^2$.

of the two quasicrystalline compounds exhibits any specific-heat anomaly at elevated temperatures that would indicate a phase transition similar to the one observed in the 1/1 Zn-Sc approximant (occurring due to freezing of the central Zn_4 tetrahedron reorientations).

The low-temperature specific heat of the i-Zn-Ag-Sc pure quasicrystal is analyzed in the inset of Fig. 8(b) in a C/T versus T^2 plot. The analysis (solid line) has yielded $\gamma = 0.90\,\mathrm{mJ/mol\,K^2}$ and $\beta_3 = 0.17\,\mathrm{mJ/mol\,K^4}$, wherefrom the Debye temperature $\theta_D = 224\,\mathrm{K}$ is obtained. The low-temperature specific heat of the i-Zn-Ag-Sc-Tm substituted compound is analyzed in the main panel of Fig. 8(b) in a C versus T scale. The theoretical curve [solid curve in Fig. 8(b)] was obtained by the set of fit parameters $B_2^0/k_B = -(3.4 \pm 0.2) \times 10^{-2}\,\mathrm{K}$, $\gamma = 20 \pm 5\,\mathrm{mJ/mol\,K^2}$, and $\beta_3 = 0.21 \pm 0.02\,\mathrm{mJ/mol\,K^4}$ (yielding $\theta_D = 210 \pm 7\,\mathrm{K}$). The $C_{\rm Sch}$, $C_{\rm el}$, and $C_{\rm latt}$ contributions to the total specific heat are also shown separately in Fig. 8(b). Around the $C_{\rm Sch}$ maximum at 0.8 K, the Schottky contribution prevails over the sum $C_{\rm el} + C_{\rm latt}$, accounting for about 85% of the total specific heat. The theoretical total specific heat curve again does not reproduce satisfactory the experimental data below the $C_{\rm Sch}$ maximum, where it decays faster than the experimental data. This discrepancy is even slightly larger than for the 1/1 Zn-Sc-Tm approximant. One of the reasons for the worse matching of the theory to the experiment in the quasicrystal as compared to the approximant could be the fact that the employed CF Hamiltonian was derived for the RE atoms located on the icosahedron of the basic three-shell cluster of the structure. In the approximant, all RE atoms are located on the icosahedra (i.e., all of them occupy the same crystallographic site), while in the i-QC, majority of the RE atoms occupy this site, whereas some are located in the glue that fills the gaps between the clusters, for which the first coordination shell does not possess the symmetry of the crystallographic site on the icosahedron. Our CF Hamiltonian is thus valid (at least approximately) for all Tm atoms in the 1/1 Zn-Sc-Tm substituted approximant, whereas in the i-Zn-Ag-Sc-Tm substituted quasicrystal it is valid for about 70% of the Tm atoms, thus making the

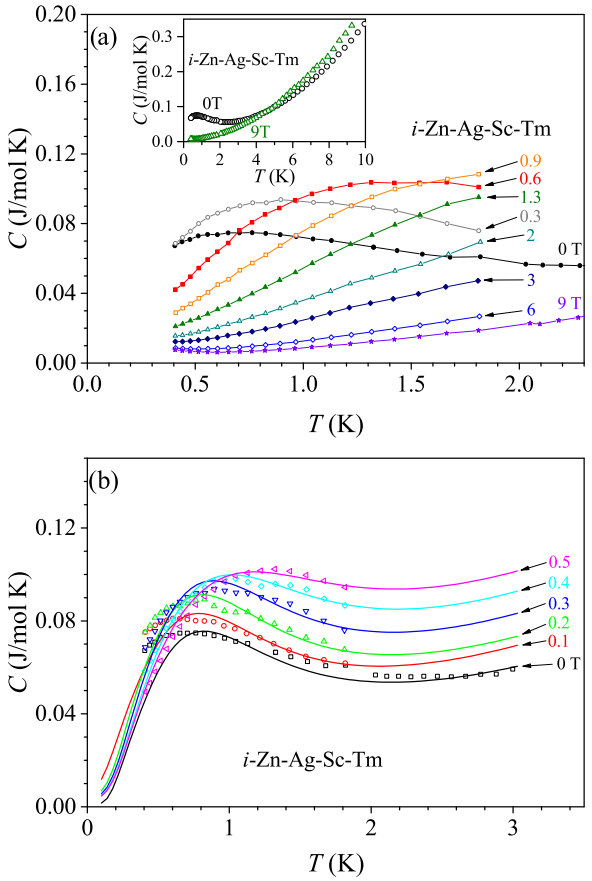

FIG. 9. (a) Low-temperature specific heat of the i-Zn-Ag-Sc-Tm quasicrystal in a magnetic field for a selected set of field values (indicated on the graph). The inset shows the specific heat in zero field and in a 9 T field in a larger temperature interval up to 10 K. (b) The specific heat in the low-field region at $B = 0$, 0.1, 0.2, 0.3, 0.4, and 0.5 T. Theoretical fits (solid curves) were obtained by the analytical model, where the Zeeman interaction is a perturbation of the CF term as expressed by Eq. (21).

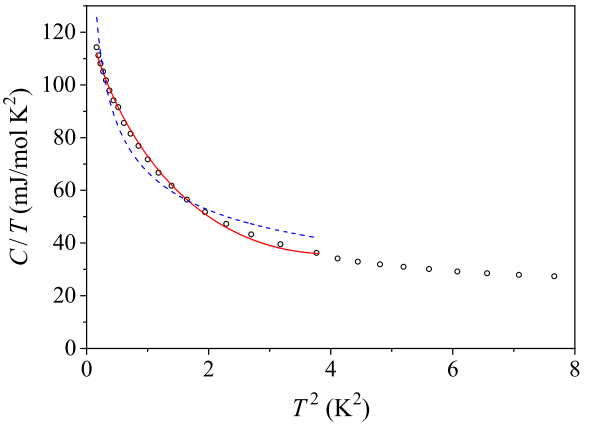

FIG. 10. Low-temperature zero-field specific heat of the 1/1 Zn-Sc-Tm "Schottky" system in a C/T versus T^2 scale. Solid curve is the fit with the expression $C/T = \gamma + AT^2\ln(T/T_{sf})$, valid for an exchange-enhanced system (the fit parameters of the curve are $\gamma = 127.7$ mJ/mol K^2, $A = 46$ mJ/mol K^4, and $T_{sf} = 3.3$ K). Dashed curve is the fit with a power-law function $C/T = BT^{-n}$[the fit parameters of the curve are $B = 66.9$ mJ/mol K^2 (where the temperature is considered to be dimensionless) and $n = 0.7$], as used in the study of quantum critical phenomena arising from strongly correlated $4f$ electrons in Fermi-liquid systems.

employed theoretical model for the C_{Sch} calculation in the latter case less applicable.

The low-temperature specific heat of the i-Zn-Ag-Sc-Tm quasicrystal in a magnetic field is shown in Fig. 9(a). The maximum due to the C_{Sch} term is again shifted to higher temperatures with increasing field and for fields larger than 1.0 T, it has already moved outside of the presented temperature interval. The specific heat in zero field and in a 9 T field in a larger temperature interval up to 10 K is shown in the inset of Fig. 9(a). The crossover between the zero field and the 9-T data due to the magnetic-field induced shift of the C_{Sch} maximum to higher temperatures occurs in the quasicrystal at about 4.5 K, which is a bit lower than in the approximant. Theoretical fits of the total specific heat in the low-field region up to 0.5 T, by using the same analytical steps as in the case of the approximant, are shown in Fig. 9(b). The field-induced shift of the Schottky peak to higher temperatures is theoretically well reproduced. The nuclear Schottky effect is also observed in the i-Zn-AgSc-Tm quasicrystal as the low-temperature upturn in the total specific heat, best observed in the specific heat data taken in external magnetic fields higher than 5 T [Fig. 7(b)].

V. DISCUSSION

We have demonstrated that the specific heat of the 1/1 Zn-Sc-Tm approximant and the i-Zn-Ag-Sc-Tm icosahedral quasicrystal contains the Schottky specific heat term, which becomes the dominant contribution to the total specific heat in the low-temperature limit at about 1.0 K and below. The presence of the Schottky term makes extraction of the electronic and lattice specific heat coefficients γ and β_3 uncertain, so that trustworthy values of these parameters cannot be derived from the analysis. Since the Schottky effect is frequently present in solids containing RE elements, the interpretation of low-temperature electronic properties of the RE-containing quasicrystals from the electronic specific heat in the $T \to 0$ limit should be done with great care.

In metallic systems it is customary to analyze the low-temperature specific heat in a C/T versus T^2 scale, which for nonmagnetic metals and alloys in the absence of the Schottky contribution ($C_{Sch} = 0$) yields a straight line $C/T = \gamma + \beta_3 T^2$, according to Eq. (14). In the presence of the Schottky contribution, the specific heat data presented in this scale show a low-temperature upturn. This is demonstrated in Fig. 10 on the example of the 1/1 Zn-Sc-Tm approximant, where the zero-field specific heat is shown in such kind of a plot. In metallic systems with incompletely filled d or f shells, electron-electron exchange interactions may provide another term to the specific heat that also produces a low-temperature upturn in the C/T versus T^2 scale. Such systems are known as the exchange-enhanced systems [44] and show instability to magnetism, i.e., they are close to a phase transition between a paramagnetic and a magnetically ordered phase. The interacting electrons give rise to long-lived spin fluctuations (similar to spin waves), which in the quantized form are called paramagnons or virtual magnons. The interaction of

the electrons with paramagnons gives rise to an enhanced effective mass of the electrons (manifested in an increased γ value) and a logarithmic term in the electronic specific heat at low temperatures, which can be represented by a general equation of the form [44]

$$C = \gamma T + AT^3 \ln(T/T_{sf}) + \beta_3 T^3, \tag{25}$$

where T_{sf} is the spin fluctuation temperature. The logarithmic term is negative for $T < T_{sf}$, so that the total specific heat shows an upturn at low temperatures when plotted as C/T versus T^2. The logarithmic term in the electronic specific heat was derived also without invoking the idea of paramagnons; it was found in ^{3}He due to temperature-dependent interparticle interaction [45] suggesting that the $T^3 \ln T$ behavior of the low-temperature specific heat may be a general feature of the Fermi-liquid systems.

In order to demonstrate the difficulty of distinguishing between the Schottky effect and the electron-electron interactions when analyzing the low-temperature upturn in the specific heat of our investigated Tm-containing quasicrystal and its approximant, we present in Fig. 10 the fit of the zero-field specific heat of the 1/1 Zn-Sc-Tm "Schottky" system with Eq. (25) rewritten in the form $C/T = \gamma + AT^2 \ln(T/T_{sf})$, valid for an exchange-enhanced system. The fit is shown by a solid curve (the fit parameters are given in the figure caption), where it is seen that the logarithmic term reproduces excellently the low-temperature upturn due to the Schottky effect in a limited temperature interval. The low-temperature upturn can also be reproduced qualitatively by a power-law function of a form $C/T = BT^{-n}$(with $n > 0$), as used in the study of quantum critical phenomena arising from strongly correlated $4f$ electrons in Fermi-liquid systems, where the zero-field C/T diverges as a power law in the $T \to 0$ limit [24]. The fit of the 1/1 Zn-Sc-Tm C/T data with the power-law function is shown in Fig. 10 as a dashed curve (the fit parameters are given in the figure caption), where it is evident that it qualitatively reproduces the low-temperature upturn. The analysis of the low-temperature specific heat of RE-containing quasicrystals and approximants may thus be ambiguous, as the Schottky effect and the electron-electron interactions both yield a very similar upturn in the C/T versus T^2 scale.

The origin of the upturn can be unraveled from the magnetic-field dependence of the low-temperature specific heat, where the Schottky effect (a single-ion property in a system of noninteracting electrons) and the electron-electron interactions in an exchange-enhanced system yield different behavior. This issue is elaborated in the Supplemental Material (see Fig. S2), where the specific heat of the 1/1 Zn-Sc-Tm quasicrystalline approximant is compared to the specific heat of the $YbCu_{4.25}$ heavy-fermion compound, belonging to the class of strongly correlated systems.

VI. CONCLUSIONS

The low-temperature electronic properties of quasicrystals remain an interesting open question with regard to the nature of the electronic state at $T = 0$, where the wave function can either be extended, localized, or critical, i.e., localized on an intermediate scale over many interatomic distances. The phenomena arising from electron-electron interactions between the $4f$ electrons and the conduction electrons in RE-containing quasicrystals are another incompletely solved problem. The purpose of this paper was to show that extraction of the electronic properties of RE-containing quasicrystals from their low-temperature specific heat may be uncertain in the presence of the Schottky effect. We have first derived the CF Hamiltonian pertinent to the class of Tsai-type icosahedral quasicrystals and their approximants, which includes most of the known RE-containing quasicrystalline systems. In the Tsai-type atomic clusters, the RE elements are located on fivefold axes of an icosahedron, so that we have derived the CF Hamiltonian for the pentagonal symmetry of the crystalline electric field. Using the leading term of this Hamiltonian, we have calculated analytically the Schottky specific heat in the presence of an external magnetic field and made comparison to the experimental specific heat of the i-Zn-Ag-Sc-Tm icosahedral quasicrystal and its 1/1 Zn-Sc-Tm approximant, both being classified as "Schottky" systems. We also show that even the nuclear Schottky effect, being much smaller effect than the ionic Schottky effect, was observed experimentally in the specific heat of the i-Zn-Ag-Sc-Tm and 1/1 Zn-Sc-Tm at $T \to 0$.

APPENDIX

The nuclear Schottky effect originates from the discrete energy levels of the RE-ion nuclear magnetic dipole moment experiencing a large effective magnetic field B_{eff} arising from the orbiting $4f$ electrons. The nuclear Schottky effect produces another specific heat contribution C^n_{Sch} that adds to Eq. (14) [42]. In the lanthanide series, the field produced by the $4f$ electrons at the position of the atomic nucleus can be enormous, well in excess of 300 T in a number of cases. In addition, the nuclear electric quadrupole moment couples to the electric field gradient (EFG) of the surrounding charges in the lattice, which also affects the energies of the discrete set of nuclear energy levels. In the case of the Tm nuclei, the ^{169}Tm isotope (of 100% natural abundance) possesses nuclear spin $I = 1/2$, so that the nuclear charge distribution is spherically symmetric and the nuclear electric quadrupole interaction vanishes. The Zeeman interaction between the nuclear magnetic moment $\vec{\mu}_n = \gamma_n \hbar \vec{I}$ (where γ_n is the nuclear gyromagnetic ratio and $\vec{I}$ is the nuclear spin operator) and $\vec{B}_{eff}$ then produces two energy levels with the splitting $\delta_n = (\varepsilon_{-1/2} - \varepsilon_{1/2})/k_B = \gamma_n \hbar B_{eff}/k_B$. The Schottky specific heat of a two-level system is given by Eqs. (17a) and (17b). Due to the smallness of δ_n, the high-temperature limit $T \gg \delta_n$ applies within the investigated range of temperatures down to 0.4 K in our experiments, so that the nuclear Schottky specific heat term will assume the asymptotic form

$$C^n_{Sch} \approx R\left(\frac{\delta_n}{2T}\right)^2, \tag{A1}$$

i.e., only the "high-temperature" decaying tail $C^n_{Sch} \propto T^{-2}$ might be observed experimentally.

[1] See, e.g., P. Fulde, in *Handbook on the Physics and Chemistry of Rare Earths*, edited by K. A. Gschneidner Jr. and L. Eyring (North-Holland, Amsterdam, 1978), Chap. 17.

[2] See, e.g., A. Tari, *The Specific Heat of Matter at Low Temperatures* (Imperial College Press, London, 2003), p. 249.

[3] D. Gignoux, F. Givord, and R. Lemaire, Phys. Rev. B **12**, 3878 (1975).

[4] O. Vogt and B. R. Cooper, J. Appl. Phys. **39**, 1202 (1968).

[5] M. T. Hutchings, in *Solid State Physics*, edited by F. Seitz and D. Turnbull (Academic, New York, 1964), Vol. 16, p. 227.

[6] A. Abragam and B. Bleaney, *Electron Paramagnetic Resonance of Transition Ions* (Clarendon, Oxford, 1970), Appendix B.

[7] K. R. Lea, M. J. M. Leask, and W. P. Wolf, J. Phys. Chem. Solids **23**, 1381 (1962).

[8] E. Segal and W. E. Wallace, J. Solid State Chem. **2**, 347 (1970).

[9] E. Segal and W. E. Wallace, J. Solid State Chem. **6**, 99 (1973).

[10] E. Segal and W. E. Wallace, J. Solid State Chem. **11**, 203 (1974).

[11] E. Segal and W. E. Wallace, J. Solid State Chem. **13**, 201 (1975).

[12] E. Segal and W. E. Wallace, *Rare Earth Intermetallics* (Academic, New York, 1973).

[13] U. Walter, Phys. Rev. B **36**, 2504 (1987).

[14] U. Walter, Europhys. Lett. **4**, 1285 (1987).

[15] A. P. Tsai, J. Q. Guo, E. Abe, H. Takakura, and T. J. Sato, Nature (London) **408**, 537 (2000).

[16] J. Q. Guo, E. Abe, and A. P. Tsai, Phys. Rev. B **62**, R14605 (2000).

[17] H. Takakura, C. P. Gómez, A. Yamamoto, M. de Boissieu, and A. P. Tsai, Nat. Mater. **6**, 58 (2007).

[18] S. Kashimoto, R. Maezawa, Y. Kasano, T. Mitani, and T. Ishimasa, Jpn. J. Appl. Phys. **42**, L1268 (2003).

[19] R. Maezawa, S. Kashimoto, and T. Ishimasa, Philos. Mag. Lett. **84**, 215 (2004).

[20] T. Ishimasa, Y. Tanaka, and S. Kashimoto, Philos. Mag. **91**, 4218 (2011).

[21] J. Q. Guo and A. P. Tsai, Philos. Mag. Lett. **82**, 349 (2002).

[22] M. Bobnar, S. Vrtnik, Z. Jagličić, M. Wencka, C. Cui, A. P. Tsai, and J. Dolinšek, Phys. Rev. B **84**, 134205 (2011).

[23] S. Jazbec, S. Vrtnik, Z. Jagličić, S. Kashimoto, J. Ivkov, P. Popčević, A. Smontara, H. J. Kim, J. G. Kim, and J. Dolinšek, J. Alloys Compd. **586**, 343 (2014).

[24] K. Deguchi, S. Matsukawa, N. K. Sato, T. Hattori, K. Ishida, H. Takakura, and T. Ishimasa, Nat. Mater. **11**, 1013 (2012).

[25] S. Kashimoto, C. Masuda, S. Motomura, S. Matsuo, and T. Ishimasa, Philos. Mag. **87**, 2929 (2007).

[26] A. I. Goldman, T. Kong, A. Kreyssig, A. Jesche, M. Ramazanoglu, K. W. Dennis, S. L. Bud'ko, and P. C. Canfield, Nat. Mater. **12**, 714 (2013).

[27] A. Niikura, A. P. Tsai, A. Inoue, and T. Masumoto, Philos. Mag. Lett. **69**, 351 (1994).

[28] T. J. Sato, Acta Crystallogr. Sect. A **61**, 39 (2005).

[29] R. I. Andrusyak, B. Ya. Kotur, and V. E. Zavodnik, Kristallografiya **34**, 996 (1989).

[30] A. Palenzona, J. Less-Common Met. **25**, 367 (1971).

[31] C. P. Gómez and S. Lidin, Angew. Chem. Int. Ed. Engl. **40**, 4037 (2001).

[32] S. Kenzari, V. Demange, P. Boulet, M. C. de Weerd, J. Ledieu, J. M. Dubois, and V. Fournée, J. Phys.: Condens. Matter **20**, 095218 (2008).

[33] P. Koželj, S. Jazbec, S. Vrtnik, A. Jelen, J. Dolinšek, M. Jagodič, Z. Jagličić, P. Boulet, M. C. de Weerd, J. Ledieu, J. M. Dubois, and V. Fournée, Phys. Rev. B **88**, 214202 (2013).

[34] H. R. Sharma, G. Simutis, V. R. Dhanak, P. J. Nugent, C. Cui, M. Shimoda, R. McGrath, A. P. Tsai, and Y. Ishii, Phys. Rev. B **81**, 104205 (2010).

[35] M. R. Li, S. Hovmöller, J. L. Sun, X. D. Zou, and K. H. Kuo, J. Alloys Compd. **465**, 132 (2008).

[36] K. W. H. Stevens, Proc. Phys. Soc. London Sect. A **65**, 209 (1952).

[37] S. Kashimoto and T. Ishimasa, in *Topology in ordered phases, Proceedings of the 1st International Symposium on TOP, Sapporo, Japan, 2005*, edited by S. Tanda, T. Matsuyama, M. Oda, Y. Asano, and K. Yakubo (World Scientific, Singapore, 2006), pp. 145–150.

[38] T. Ishimasa, Y. Kaneko, and H. Kaneko, J. Non-Cryst. Solids **334-335**, 1 (2004).

[39] W. B. Pearson, *The Crystal Chemistry and Physics of Metals and Alloys* (Wiley-Interscience, New York, 1972).

[40] See Supplemental Material at http://link.aps.org/supplemental/10.1103/PhysRevB.93.054208 for the electrical resistivity measurements and comparison of the Schottky specific heat to that of an exchange-enhanced system.

[41] F. E. Mabbs and D. J. Machin, *Magnetism and Transition Metal Complexes* (Chapman and Hall, London, 1973), p. 7.

[42] A. Tari, in Ref. 2, Chap. 6.

[43] See, for a review, K. Binder and A. P. Young, Rev. Mod. Phys. **58**, 801 (1986).

[44] K. Ikeda, S. K. Dhar, M. Yoshizawa, and K. A. Gschneidner Jr., J. Magn. Magn. Mater. **100**, 292 (1991).

[45] D. N. Tripathi and S. Mishra, Physica B **226**, 338 (1996).